J. MAGNETISM AND MAGNETIC MATERIALS

IMPACT FACTOR = 3.097

www.sciencedirect.com/journal/journal-of-magnetism-and-magnetic-materials

Accepted October 28th 2022

Electro-magnetohydrodynamics hybrid nanofluid flow with Gold and Magnesium oxide nanoparticles through vertical parallel plates

M. M. Bhatti[a], O. Anwar Bég[b], R. Ellahi[c,d,e,1], M. H. Doranehgard[f], Faranak Rabiei[g]

[a]College of Mathematics and Systems Science, Shandong University of Science and Technology, Qingdao 266590, Shandong, China.
[b] Multi-Physical Engineering Sciences Group, Mechanical Engineering, Salford University, School of Science, Engineering and Environment (SEE), Manchester, M54WT, UK.
[c] Center for Modeling & Computer Simulation, Research Institute, King Fahd University of Petroleum & Minerals, Dhahran-31261, Saudi Arabia
[d] Department of Mathematics and Statistics, International Islamic University, Islamabad, Pakistan
[e] Fulbright Fellow Department of Mechanical Engineering University of California Riverside, USA [f]Department of Civil and Environmental Engineering, University of Alberta, Edmonton, Alberta T6G 1H9, Canada
[g]School of Engineering, Monash University Malaysia, 47500, Selangor, Malaysia

Abstract: The hybrid nanofluid flow under suspension of Gold and Magnesium oxide nanoparticles (Au/MgO-NPs) propagating between vertical parallel plates is investigated. Sodium alginate third-grade non-Newtonian fluid is used as the base fluid. The effect of electro-magnetohydrodynamics is also taken into account. The energy equation also includes the effect of Joule heating and viscous dissipation. Due to the nonlinear nature of the formulated differential equations, perturbation strategy is utilized to acquire the analytical solutions. Discussion and plotting are presented with respect to most significant parameters. It is analyzed that the rate of heat transfer is dramatically increased, and this is owing to an increase in the thermal conductivity of the fluid due to hybrid nanofluid.

[1] Corresponding author, (R. Ellahi): E-mails: rahmatellahi@yahoo.com; rellahi@alumni.ucr.edu,

With increment in buoyancy convection parameter and electric field parameter, the flow is accelerated. It is also noted that the temperature is boosted with increasing nanoparticle volume fraction of both magnesium oxide and gold nanoparticles. A comparison with previously studied results is also included. The applications of the work include novel thermal duct processing technologies in biomedical, nuclear and process engineering.

Keywords: Hybrid nanofluid; Electro-magnetohydrodynamics; Thermal buoyancy; Gold and Magnesium oxide nanoparticles.

1. Introduction

Energy is a huge quantity of information that can be transmitted from one device to another to execute tasks. It can be done with heat or with work [1]. When there is a temperature difference among two systems, heat can be transferred from one to the other and propagate from a higher to a lower temperature region [2]. Heat transfer is the term used to describe the process of transferring heat (thermal) energy from one system to another. Heat transfer applications have become commonplace in our daily lives [3-7] for example, the human body produces heat and adjusts its temperature in response to the surroundings by wearing clothing. Heat transfer is also used to regulate the temperature in our homes and offices, and it is required for drying, cooking, and refrigeration. Heat transfer is also used in automobile radiators, electronic devices, solar thermal collectors (which transmute solar energy into power and heat), and spacecraft. Heat must be dissipated quickly in these types of devices in order for the system to execute and operate properly. Due to recent technological advancements, increasingly device sizes are being reduced (miniaturization) with a thrust towards improved heat management. Therefore, heat transfer augmentation is extremely important in the field of thermal engineering.

To enhance the heat transfer coefficient between working fluids, a variety of approaches have been developed [8, 9]. For example, the suspension of solid particles (nanosized) in a base fluid has been shown to improve the thermal characteristics of the base fluid. Choi and Eastman [10] were the first one to describe this type of fluid, which they termed nanofluids. Nanofluids can be prepared by dispersing small metallic oxide particles, metallic or carbon-based components in the working fluids. Recently, new class of nanofluids have been introduced which is known as hybrid nanofluids. Hybrid nanofluids are a novel type of fluid that has emerged in recent years. The suspension of two or more types of nanoparticles in a base fluid can create hybrid nanofluids. The nanoparticles contained in the base fluid are exceedingly small (approximately less than 100 nm), making this type of working fluid ideal for heat transfer applications. Different types of conventional fluids can be used as hybrid nanofluid such as water, Ethylene glycol, paraffin oil, engine oil, vegetable oil, kerosene, Sodium alginate, and water-ethylene glycol mixture etc. The following nanoparticles are utilized to improve heat transfer for working fluids: diamond-Ni, MgO-MWCNT, SiO2-CNT, SWCNT-MgO, Ag-TiO2, Ta-Ni, Ag-MnO, Al2O3-Ag, Cu-Zn, Ag-SiO-carbon, Graphene-Ag, MWCNT-Fe3O4, Cu–TiO2, Al2O3-SiO2, Ag-CNT, Fe3O4-Graphene, Al2O3-MEPCM, Al2O3-CNT, Fe2O3-CNT, ND-Co3O4 etc. Hybrid nanofluids have been employed in a variety of heat transfer applications [11-13], including micro-channels, plate heat exchangers, pipelines, air-conditioning systems, tube and shell heat exchangers, tabular heat exchangers, tube-in-tube heat exchangers, thermal ducts, helical coils and coiled heat exchangers. Kumar et al. [14] presented a detailed applications of multiple hybrid nanofluids using carreau fluid. Hybrid nanofluid with Cattaneo–Christov heat flux model was examined by Reddy et al. [15]. Recently, Reddy et al. [16] studied the magnetized hybrid nanofluids over a rotating disk in the presence of Arrhenius kinetics.

Magnesium oxide nanoparticles (MgO-NPs) [17] have attracted a significant amount of attention to their multidimensional applications when compared to other nanoparticles in a variety of fields such as biomedical engineering, catalysis, refractory materials, glass industry, pharmaceuticals, waste remediation and heat transfer applications. These materials are extremely advantageous since they offer exceptional features such as an excellent strength-to-weight ratio, recycling activity, good functionality, hygroscopic nature, and low density. MgO-NPs have a wide range of applications due to their properties, which include cost-effective manufacturing, a higher melting point, biocompatibility, and biodegradability. Kumaresan et al. [18] investigated magnetic copper and magnesium oxide nanoparticles in the presence of heat generation, absorption, and thermal radiation in transport in a porous medium. Pandiaraj et al. [19] used flat plate heat pipes to investigate magnesium oxide nanoparticles with statistical analyses. Khodadadi et al. [20] analyzed the performance of nanoparticles on the analysis of magnesium oxide nanoparticles suspended in water and provided a statistical model. The behavior of magnesium oxide nanoparticles floating in the heat pipe solar collector was studied experimentally by Dehaj and Mohiabadi [21]. The stability of magnesium oxide nanoparticles and their thermal performance in a flat plate solar collector were discussed by Chaudhry et al. [22]. The effect of an inclined magnetic field on the free convection flow of MoS2 and MgO nanoparticles suspended in water and floating on the surface of a porous elastic surface was studied by Hymavathi et al. [23]. Reddy and Shehzed [24] computed the transport of micropolar fluid doped with magnesium oxide and molybdenum disulfide nanoparticles also using a Catteno-Christov heat flux model.

On the other hand, gold nanoparticles (Au-NPs) have also many applications [25-27] in biomedical engineering, electronics, therapeutic agent delivery, probes, catalysis, photodynamic therapy, sensors, and diagnostics etc. Gold nanoparticles exhibit a number of desirable properties [28] including a high surface-to-volume ratio, low toxicity, size and

shape-dependent optoelectronics properties, and remarkable biocompatibility. Beicker et al. [29] analyzed photothermal conversion using gold nanoparticles and multi-walled carbon nanotubes floating in water by experimental analysis. Elgazery [30] adopted a non-Newtonian fluid model with alumina and gold nanoparticles in a non-Darcy porous medium with magnetohydrodynamic effect. Dinarvand and Rostami [31] investigated the von Karman swirling flow using a mass-based model and a hybrid nanofluid containing gold and zinc oxide nanoparticles. Rashid et al. [32] explored gold nanoparticle structure effects and heat transport in parallel plate squeezing channel flow. The boundary layer flow of gold-thorium water-based nanofluids propagating through semi-infinite plat was studied by Govindaraju and Selvaraj [33]. Yin et al. [34] provided numerical results for the heat radiation impact on molybdenum/gold water-based hybrid nanofluids under convective conditions. The references list (see refs. Verma et al. [35]; Ghalambaz et al. [36]; Saba et al. [37]; Basha et al. [38]; Zhang et al. [39]) contains a number of other noteworthy studies that are relevant to hybrid nanofluid dynamics.

The primary goal of this research is to investigate the electro-magneto-hydrodynamic (EMHD) hybrid nanofluid flow in a vertical parallel plate channel filled with sodium alginate third-grade fluid with gold and magnesium oxide nanoparticles. A transverse magnetic and axial electrical field are considered. In thermo-bioengineering, magnetic nanoparticles [40-42] offer a wide range of applications. The position of magnetic nanoparticles can be manipulated using magnets with carefully controlled external magnetic field. The use of a variable magnetic field to heat nanoparticles is advantageous, and magnetic nanoparticles can also be utilized as a contrast agent in magnetic resonance imaging. The mathematical modeling is based on the momentum equation, the energy equation (modified with Ohm's law) and featuring viscous dissipation. Using a perturbation scheme, the formulated differential equations are solved analytically, subject to physically appropriate boundary

conditions, and the solutions up to second order are derived. Graphs and tables are used to illustrate and explain the effects of all of the parameters under consideration. A comparison is also presented to validate the current model and verify that the present results for novel hybrid nanofluid are correct. The novelty of the present work is the *simultaneous consideration of both magnetic and electric fields, nanofluid rheology and gold/magnesium oxide nanoparticles* which has not been addressed previously in the literature.

Nomenclature

$\vec{V}$	Velocity vector (m/s)
T	Temperature (K)
G	Gravity (m/s^2)
T_m	Mean temperature (K)
p'	Pressure (Pa)
t'	Time (s)
$\vec{B}$	Magnetic field (Tesla)
$\vec{J}$	Local ion current density vector (A/m^2)
$\vec{E}$	Electrical field (V/m)
k	Thermal conductivity (W·m^{-1}·K^{-1})
c_p	Specific heat (J·kg^{-1}·K^{-1})
Gr	Thermal Grashof number
Re	Reynolds number
S	Skin friction coefficient
h	Nusselt number

Greek letters

τ'	Stress tensor (N/m^2)
μ	Viscosity (Pa s)
β	Thermal expansion coefficient (K^{-1})
ρ	Density (kg/m^3)
σ	Electrical conductivity (S/m)
$\tau_1, \tau_2, \overline{\tau}_1, \overline{\tau}_2, \overline{\tau}_3$	Material constants
γ	Hartmann number
ξ	Electrical strength parameter
χ	Third-grade non-Newtonian (viscoelastic) fluid parameter
θ	Buoyancy convection parameter
δ	Brinkman number
β_2	Joule heating parameter
β_1	Heat generation owing to the interaction of magnetic and electric fields
ψ_1	Volume fraction of Mgo nanoparticles
ψ_2	Volume fraction of Au nanoparticles

Abbreviations:

SA	Sodium alginate
MgO	Magnesium oxide
Au	Gold
NPs	Nanoparticles
hnf	Hybrid nanofluid

2. Formulation of the Problem

Let us consider the Sodium Alginate (SA) third-grade hybrid nanofluid flow between two vertical parallel plates (channel) located at a finite distance 2λ. The fluid is electrically conducting and incompressible and both axial electric and transverse magnetic field are present. The base fluid contains magnesium oxide and gold nanoparticles (MgO/Au-NPs). It is presumed that the base fluid and nanoparticles are in thermal equilibrium and that no slip arises between them. A Cartesian coordinate system is adopted. The walls of the channel (duct) located at $x=\lambda$ and $x=-\lambda$ are held at a constant temperatures T_2 and T_1, where $T_1 > T_2$. Based on the proposed assumptions, the continuity equation is expressed as:

$$\nabla \cdot \vec{\mathrm{V}} = 0, \tag{1}$$

The momentum equation using Ohm's law is defined as [43]:

$$\rho_{hnf}\left(\vec{\mathrm{V}}\cdot\nabla\vec{\mathrm{V}} + \frac{\partial\vec{\mathrm{V}}}{\partial t'}\right) = -\nabla\cdot p' + \nabla\tau' + \vec{\mathrm{J}}\times\vec{\mathrm{B}} + \left(\rho\beta\right)_{hnf}\left(T - T_m\right)g, \tag{2}$$

Here the stress tensor is denoted by τ', viscosity is denoted by μ, pressure is denoted by p', g is the gravity, thermal expansion coefficient is denoted by β, T is the temperature, $T_m\left[=\left(T_1+T_2\right)/2\right]$ is the mean temperature, density is denoted by ρ, *hnf* in subscript denotes the hybrid nanofluid; time is denoted by t', magnetic field is denoted by $\vec{\mathrm{B}}$, and local ion current density vector is denoted by $\vec{\mathrm{J}}$ and it is defined as:

$$\vec{\mathrm{J}} = \sigma_{hnf}\left(\vec{\mathrm{V}}\times\vec{\mathrm{B}} + \vec{\mathrm{E}}\right), \tag{3}$$

Here electrical conductivity is denoted by σ, and electrical field is denoted by $\vec{\mathrm{E}}$.

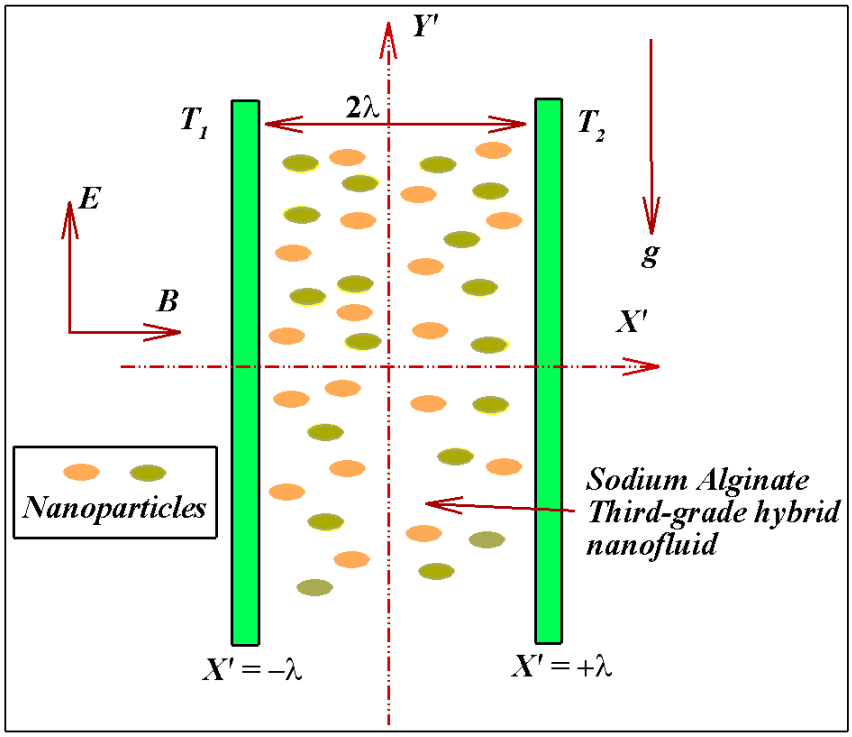

Figure 1: Geometrical structure of the hybrid nanofluid flow through a vertical parallel plate channel.

The constitutive equation for a third-grade Reiner-Rivlin differential viscoelastic fluid [44] is defined as:

$$\tau' = \mu_{hnf}\hbar_1 + \tau_1\hbar_2 + \tau_2\hbar_1^2 + \overline{\tau}_1\hbar_3 + \overline{\tau}_2\left(\hbar_1\hbar_2 + \hbar_2\hbar_1\right) + \overline{\tau}_3\left(\mathrm{tr}\hbar_1^2\right)\hbar_1, \tag{4}$$

Where $\tau_1, \tau_2, \overline{\tau}_1, \overline{\tau}_2, \overline{\tau}_3$ represents the material constants, and the kinematical tensors $\hbar_1, \hbar_2, \hbar_3$ are expressed as

$$\begin{cases} \hbar_1 = \mathrm{X} + \mathrm{X}^{\mathrm{t}}, \qquad \mathrm{X} = \nabla\cdot\vec{\mathrm{V}}, \\ \hbar_n = \dfrac{\mathrm{d}\hbar_{n-1}}{\mathrm{d}t'} + \mathrm{X}^{\mathrm{t}}\hbar_{n-1} + \hbar_{n-1}\mathrm{X}, \qquad n = 2,3,\ldots \end{cases} \tag{5}$$

If the model is compatible with thermodynamics such that the all the fluid motions meet the *Clausius-Duhem inequality*, and the assumption of the specific Helmholtz free energy be a minimum in equilibrium then the following conditions are defined as:

$$\mu \geq 0, \quad \tau_1 \geq 0, \quad \left|\tau_1 + \tau_2\right| \leq \sqrt{24\mu\overline{\tau}_3}, \quad \overline{\tau}_1 = \overline{\tau}_2 = 0, \quad \overline{\tau}_3 \geq 0. \tag{6}$$

The energy equation with viscous dissipation and the Joule heating effects are described as:

$$\left(\rho c_p\right)_{hnf}\frac{\mathrm{d}T}{\mathrm{d}t'}=k_{hnf}\nabla\cdot T+\tau':\nabla\cdot\vec{\mathrm{V}}+\frac{\vec{\mathrm{J}}\cdot\vec{\mathrm{J}}}{\sigma_{hnf}} \tag{7}$$

where thermal conductivity of the fluid is denoted by k, c_p denotes the specific heat, and the symbols "$\cdot$" and "$:$" represents the single and double dot products.

For the proposed problem, we will seek the velocity field and the temperature field in the following form:

$$\vec{\mathrm{V}}=\left[0,V\left(X'\right),0\right],\quad T=T\left(X'\right). \tag{8}$$

Using equation (7) into the governing equation (2), we get the following set of equations:

$$\frac{\partial p'}{\partial X'}=\left(2\tau_1+\tau_2\right)\frac{\mathrm{d}}{\mathrm{d}X'}\left[\left(\frac{\mathrm{d}V}{\mathrm{d}X'}\right)^2\right], \tag{9}$$

$$\frac{\partial p'}{\partial Y'}=\mu_{hnf}\frac{\mathrm{d}^2V}{\mathrm{d}X'^2}+6\bar{\tau}_3\frac{\mathrm{d}^2V}{\mathrm{d}X'^2}\left(\frac{\mathrm{d}V}{\mathrm{d}X'}\right)^2-\sigma_{hnf}B^2V+\sigma_{hnf}BE+\left(\rho\beta\right)_{hnf}\left(T-T_m\right)g, \tag{10}$$

$$\frac{\partial p'}{\partial Z'}=0. \tag{11}$$

Defining the modified pressure in the following form

$$\hat{p}=p'-\left(2\tau_1+\tau_2\right)\left[\left(\frac{\mathrm{d}V}{\mathrm{d}X'}\right)^2\right], \tag{12}$$

In view of Eq. (11), Eqs. (8-10) can be reduced to the following form as:

$$\frac{\partial\hat{p}}{\partial X'}=0, \tag{13}$$

$$\frac{\partial\hat{p}}{\partial Y'}=\mu_{hnf}\frac{\mathrm{d}^2V}{\mathrm{d}X'^2}+6\bar{\tau}_3\frac{\mathrm{d}^2V}{\mathrm{d}X'^2}\left(\frac{\mathrm{d}V}{\mathrm{d}X'}\right)^2-\sigma_{hnf}B^2V+\sigma_{hnf}BE+\left(\rho\beta\right)_{hnf}\left(T-T_m\right)g, \tag{14}$$

$$\frac{\partial \hat{p}}{\partial Z'} = 0. \tag{15}$$

It can be seen from the previous equations that the pressure function $\partial \hat{p}/\partial Y'$ is constant. We get

$$\mu_{hnf} \frac{\mathrm{d}^2 V}{\mathrm{d}X'^2} + 6\bar{\tau}_3 \frac{\mathrm{d}^2 V}{\mathrm{d}X'^2}\left(\frac{\mathrm{d}V}{\mathrm{d}X'}\right)^2 - \sigma_{hnf} B^2 V + \sigma_{hnf} BE + (\rho\beta)_{hnf}(T - T_m)g = 0, \tag{16}$$

The velocity boundary conditions at the duct walls are defined as follows:

$$V(\pm\lambda) = 0, \tag{17}$$

For EMHD, the energy equation given in Eq. (7), in view of Eq. (8), is obtained as:

$$k_{hnf} \frac{\partial^2 T}{\partial X'^2} + \mu_{hnf}\left(\frac{\mathrm{d}V}{\mathrm{d}X'}\right)^2 + 2\bar{\tau}_3\left(\frac{\mathrm{d}V}{\mathrm{d}X'}\right)^4 + \sigma_{hnf}\left(B^2V^2 + E^2 - 2BEV\right) = 0. \tag{18}$$

The Joule heating and volumetric heat generation owing to viscous dissipation are represented by the last terms in the preceding equation.

The thermal boundary conditions are defined as follows, in accordance with the geometrical structure:

$$T(-\lambda) = T_1, \quad T(+\lambda) = T_2, \tag{19}$$

The following step involves converting the aforementioned equations into dimensionless form by employing the variables mentioned below:

$$v = \frac{V}{V_0}, X = \frac{X'}{\lambda}, T = \frac{T - T_m}{T_1 - T_2}, \tag{20}$$

Here V_0 is a reference velocity.

Using Eqn. (20), the dimensionless form of Eqns. (16) & (19) emerge as:

$$\frac{\mu_{hnf}}{\mu_f}\frac{\mathrm{d}^2 v}{\mathrm{d}x^2} + 6\chi\left(\frac{\mathrm{d}v}{\mathrm{d}x}\right)^2 \frac{\mathrm{d}^2 v}{\mathrm{d}x^2} - \frac{\sigma_{hnf}}{\sigma_f}\gamma^2 v + \xi + \theta\frac{(\rho\beta)_{hnf}}{(\rho\beta)_f}T = 0, \tag{21}$$

$$\frac{k_{hnf}}{k_f}\frac{\mathrm{d}^2T}{\mathrm{d}x^2}+\delta\frac{\mu_{hnf}}{\mu_f}\left(\frac{\mathrm{d}v}{\mathrm{d}x}\right)^2+2\delta\chi\left(\frac{\mathrm{d}v}{\mathrm{d}x}\right)^4+\frac{\sigma_{hnf}}{\sigma_f}\delta\gamma^2v^2-\frac{\sigma_{hnf}}{\sigma_f}\beta_1v+\frac{\sigma_{hnf}}{\sigma_f}\beta_2=0, \tag{22}$$

The boundary conditions (17) and (19) now assume the dimensionless form:

$$\left.\begin{aligned} v(-1)=0, \quad T(-1)=\frac{1}{2},\\ v(+1)=0, \quad T(+1)=-\frac{1}{2}, \end{aligned}\right\} \tag{23}$$

and

$$\begin{aligned} &Gr=\frac{g(\rho\beta)_f\lambda^3(T_1-T_2)}{\mu_f\upsilon_f},\mathrm{Re}=\frac{V_0\lambda}{\upsilon_f},\xi=\frac{\sigma_fBE\lambda^2}{\mu_fV_0},\chi=\frac{V_0^2\bar{\tau}_3}{\mu_f\lambda^2},\\ &\gamma=B\lambda\sqrt{\frac{\sigma_f}{\mu_f}},\theta=\frac{Gr}{\mathrm{Re}},\delta=\frac{\mu_fV_0^2}{k_f(T_1-T_2)},\beta_1=\frac{2BE\lambda^2V_0\sigma_f}{(T_1-T_2)k_f},\beta_2=\frac{\lambda^2E^2\sigma_f}{(T_1-T_2)k_f}. \end{aligned} \tag{24}$$

Here Hartmann number is denoted by γ, dimensionless parameter related to electrical strength is denoted by ξ, third-grade non-Newtonian (viscoelastic) fluid parameter is denoted by χ, buoyancy convection parameter due to temperature is denoted by θ, Gr is the thermal Grashof number, Re is the Reynolds number, δ represents the Brinkman number (which indicates the ratio of heat created by viscous dissipation to heat transferred by molecular conduction), the effects of heat generation owing to the interaction of magnetic and electric fields on heat conduction is denoted by β_1 and the ratio of Joule heating to heat conduction is represented by β_2.

The physical and thermodynamics properties of hybrid nanofluids are defined with the following relations [45,46]:

a. Density:

$$\rho_{hnf}=\rho_1^{np}\psi_1+\rho_2^{np}\psi_2+\rho_f(1-\psi_{hnf}), \quad \psi_{hnf}=\psi_1+\psi_2, \tag{25}$$

b. Heat capacity:

$$(\rho C_p)_{hnf} = (\rho C_p)_1^{np} \psi_1 + (\rho C_p)_2^{np} \psi_2 + (\rho C_p)_f (1 - \psi_{hnf}),$$

(26)

c. Dynamic viscosity:

$$\mu_{hnf} = \frac{\mu_f}{(1 - \psi_{hnf})^{2.5}},$$

(27)

d. Thermal conductivity:

$$\kappa_{hnf} = \kappa_f \times \left[\frac{2\kappa_f + \left(\frac{\psi_1 \kappa_1^{np} + \psi_2 \kappa_2^{np}}{\psi_{hnf}} \right) + 2(\psi_1 \kappa_1^{np} + \psi_2 \kappa_2^{np}) - 2\psi_{hnf} \kappa_f}{2\kappa_f + \left(\frac{\psi_1 \kappa_1^{np} + \psi_2 \kappa_2^{np}}{\psi_{hnf}} \right) - (\psi_1 \kappa_1^{np} + \psi_2 \kappa_2^{np}) + \psi_{hnf} \kappa_f} \right],$$

(28)

e. Thermal expansion coefficient:

$$(\rho\beta)_{hnf} = (1 - \psi_{hnf})(\rho\beta)_f + (\rho\beta)_1^{np} \psi_1 + (\rho\beta)_2^{np} \psi_2,$$

(29)

f. Electric conductivity:

$$\sigma_{hnf} = \left[1 + \frac{3\psi_{hnf} \left(\frac{\sigma_{hnp}}{\sigma_f} - 1 \right)}{\left(\frac{\sigma_{hnp}}{\sigma_f} + 2 \right) - \left(\frac{\sigma_{hnp}}{\sigma_f} - 1 \right) \psi_{hnf}} \right] \times \sigma_f, \quad \sigma_{hnp} = \frac{\psi_1 \sigma_1^{np} + \psi_2 \sigma_2^{np}}{\psi_{hnf}}.$$

(30)

Here ψ_1 denotes the volume fraction of MgO nanoparticles, and ψ_2 denotes the volume fraction of Au nanoparticles. The properties for the nanoparticles and Sodium Alginate (SA) third-grade base fluid are given in Table 1. The above model has been successfully used by Takabi and Salehi [46] and Tayebi and Chamkha [47] for Al_2O_3-Cu/water hybrid nanofluid in different geometrical configurations.

The skin friction coefficient and the Nusselt number on the left plate at $X' = -\lambda$ is defined in dimensionless form as:

$$\left.\begin{aligned} Cf &= \frac{\mu_{hnf}}{\mu_f}\frac{\mathrm{d}v}{\mathrm{d}x}(-1), \\ Nu &= \frac{k_{hnf}}{k_f}\frac{\mathrm{d}T}{\mathrm{d}x}(-1). \end{aligned}\right\} \tag{31}$$

3. Solution of the Problem

To obtain the solution of the resulting nonlinear differential equations (24-25), we have used homotopy perturbation method. The perturbation formulation for equations (24-25) are defined in the following form as [43]:

$$h(\bar{v},\varepsilon) = (1-\varepsilon)\left[L_0(\bar{v}) - L_0(\tilde{v}_0)\right] + \varepsilon\left[L_0(\bar{v}) + \frac{6\chi}{\Im_1}\left(\frac{\mathrm{d}\bar{v}}{\mathrm{d}x}\right)^2\frac{\mathrm{d}^2\bar{v}}{\mathrm{d}x^2} - \frac{\Im_2}{\Im_1}\gamma^2\bar{v} + \frac{\xi}{\Im_1} + \frac{\Im_3}{\Im_1}\theta\bar{T}\right], \tag{32}$$

$$h(\bar{T},\varepsilon) = (1-\varepsilon)\left[L_0(\bar{T}) - L_{\mathrm{op}}(\tilde{T}_0)\right] + \varepsilon\left[\begin{aligned} &L_0(\bar{T}) + \delta\frac{\Im_1}{\Im_4}\left(\frac{\mathrm{d}\bar{v}}{\mathrm{d}x}\right)^2 \\ &+ \frac{2\delta\chi}{\Im_4}\left(\frac{\mathrm{d}\bar{v}}{\mathrm{d}x}\right)^4 + \frac{\Im_2}{\Im_4}\left(\delta\gamma^2\bar{v}^2 - \beta_1\bar{v} + \beta_2\right) \end{aligned}\right], \tag{33}$$

and

$$\Im_1 = \frac{\mu_{hnf}}{\mu_f}, \Im_2 = \frac{\sigma_{hnf}}{\sigma_f}, \Im_3 = \frac{(\rho\beta)_{hnf}}{(\rho\beta)_f}, \Im_4 = \frac{k_{hnf}}{k_f} \tag{34}$$

We have selected the following linear operator L_0 and the initial guess $\tilde{v}_0, \tilde{\vartheta}_0$ in the following form:

$$L_{\mathrm{op}} = \frac{\mathrm{d}^2}{\mathrm{d}x^2}, \tilde{v}_0 = \frac{x^2-1}{2}, \tilde{\vartheta}_0 = -\frac{x}{2} \tag{35}$$

To continue, let us introduce the series expansion for equations (32-33), which we have.

$$\begin{aligned} \bar{v} &= \bar{v}_0 + \varepsilon\bar{v}_1 + \varepsilon^2\bar{v}_2 + \ldots, \\ \bar{T} &= \bar{T}_0 + \varepsilon\bar{T}_1 + \varepsilon^2\bar{T}_2 + \ldots, \end{aligned} \tag{36}$$

We get a set of linear differential equations at each order by substituting equation (36) into equations (32-33). After the completion of this step, we will use the symbolic computational software Mathematica to obtain the solutions of the linear differential equation at each order.

3.1 Zeroth other system ε^0

We get the following set of differential equations with boundary conditions of zeroth order:

$$\begin{aligned} &L_0\left(\bar{v}_0\right)-L_0\left(\tilde{v}_0\right)=0,\\ &v_0\left(\pm1\right)=0, \end{aligned} \tag{37}$$

$$\begin{aligned} &L_0\left(\bar{T}_0\right)-L_0\left(\tilde{T}_0\right)=0,\\ &\bar{T}_0\left(-1\right)=\frac{1}{2},\bar{T}_0\left(+1\right)=-\frac{1}{2}, \end{aligned} \tag{38}$$

The solution at the zeroth order is obtained as:

$$\left.\begin{aligned} &\bar{v}_0=\frac{x^2-1}{2},\\ &\bar{T}_0=-\frac{x}{2}, \end{aligned}\right\} \tag{39}$$

3.2 First order system ε^1

The first order system is obtained in the following form as:

$$\left.\begin{aligned} &L_0\left(\bar{v}_1\right)+L_0\left(\tilde{v}_0\right)+\frac{6\chi}{\Im_1}\left(\frac{\mathrm{d}\bar{v}_0}{\mathrm{d}x}\right)^2\frac{\mathrm{d}^2\bar{v}_0}{\mathrm{d}x^2}-\frac{\Im_2}{\Im_1}\gamma^2\bar{v}_0+\frac{\xi}{\Im_1}+\frac{\Im_3}{\Im_1}\theta\bar{T}_0,\\ &v_1\left(\pm1\right)=0, \end{aligned}\right\} \tag{40}$$

$$\left.\begin{aligned} &L_0\left(\bar{T}_1\right)+L_0\left(\tilde{T}_0\right)+\delta\frac{\Im_1}{\Im_4}\left(\frac{\mathrm{d}\bar{v}_0}{\mathrm{d}x}\right)^2+\frac{2\delta\chi}{\Im_4}\left(\frac{\mathrm{d}\bar{v}_0}{\mathrm{d}x}\right)^4+\frac{\Im_2}{\Im_4}\left(\delta\gamma^2{\bar{v}_0}^2-\beta_1\bar{v}_0+\beta_2\right),\\ &\bar{T}_1\left(\pm1\right)=0, \end{aligned}\right\} \tag{41}$$

The solution of the first order system is obtained as:

$$\bar{v}_1=\frac{\left(-1+x^2\right)\left[-12\Im_1+\Im_2\gamma^2\left(-5+x^2\right)+2\left(\Im_3\theta x-6\left(\xi+\chi+x^2\chi\right)\right)\right]}{24\Im_1}, \tag{42}$$

$$\bar{T}_1=-\frac{\left(-1+x^2\right)}{120\Im_4}\left[\begin{aligned} &10\Im_1\left(1+x^2\right)\delta+\Im_2\left\{-5\left(-5+x^2\right)\beta_1+60\beta_2+\gamma^2\left(11-4x^2+x^4\right)\delta\right\}\\ &+8\left(1+x^2+x^4\right)\delta\chi \end{aligned}\right], \tag{43}$$

3.3 Second order system ε^2

The second order system is obtained as:

$$\left.\begin{aligned} &L_0\left(\bar{v}_2\right)+\frac{6\chi}{\Im_1}\left[2\frac{\mathrm{d}\bar{v}_0}{\mathrm{d}x}\frac{\mathrm{d}^2\bar{v}_0}{\mathrm{d}x^2}\frac{\mathrm{d}\bar{v}_1}{\mathrm{d}x}+\frac{\mathrm{d}^2\bar{v}_1}{\mathrm{d}x^2}\left(\frac{\mathrm{d}\bar{v}_0}{\mathrm{d}x}\right)^2\right]-\frac{\Im_2}{\Im_1}\gamma^2\bar{v}_1+\frac{\Im_3}{\Im_1}\theta\bar{T}_1,\\ &\bar{v}_2\left(\pm1\right)=0, \end{aligned}\right\} \tag{44}$$

$$\left.\begin{aligned} &L_0\left(\bar{T}_1\right)+2\delta\frac{\Im_1}{\Im_4}\frac{\mathrm{d}\bar{v}_0}{\mathrm{d}x}\frac{\mathrm{d}\bar{v}_1}{\mathrm{d}x}+\frac{8\delta\chi}{\Im_4}\frac{\mathrm{d}\bar{v}_1}{\mathrm{d}x}\left(\frac{\mathrm{d}\bar{v}_0}{\mathrm{d}x}\right)^3+\frac{\Im_2}{\Im_4}\left(2\delta\gamma^2v_1v_0-\beta_1\bar{v}_1\right),\\ &\bar{T}_1\left(\pm1\right)=0, \end{aligned}\right\} \tag{45}$$

The solution of the second order system is obtained as:

$$\bar{v}_2=\bar{v}_{2,0}+\bar{v}_{2,1}x+\bar{v}_{2,2}x^2+\bar{v}_{2,3}x^3+\bar{v}_{2,4}x^4+\bar{v}_{2,5}x^5+\bar{v}_{2,6}x^6+\bar{v}_{2,7}x^8, \tag{46}$$

$$\bar{T}_2=\bar{T}_{2,0}+\bar{T}_{2,1}x+\bar{T}_{2,2}x^2+\bar{T}_{2,3}x^3+\bar{T}_{2,4}x^4+\bar{T}_{2,5}x^5+\bar{T}_{2,6}x^6+\bar{T}_{2,7}x^7+\bar{T}_{2,8}x^8, \tag{47}$$

The constants $v_{1,n},\vartheta_{1,n};\left(n=0,1\ldots,6\right)$ mentioned in the above equations are given in Appendices A and B.

Using the HPM property, we may derive the final form of the solutions as:

$$v=\lim_{\varepsilon\to1}\bar{v}=\bar{v}_0+\bar{v}_1+\bar{v}_2+\ldots, \tag{48}$$

$$T=\lim_{\varepsilon\to1}\bar{T}=\bar{T}_0+\bar{T}_1+\bar{T}_2+\ldots, \tag{49}$$

4. Results and discussion

Extensive visualizations of the impact of numerous emerging physical parameters on transport characteristics are presented. Specifically, graphical results for the velocity profile, the skin friction coefficient, the temperature profile, and the Nusselt number in particular. The linear differential equations at each order solved with the help of *DSolve* command in *Mathematica*. The following parametric values have been chosen to proceed with graphical

computations, for instance: $\delta = 0.5, \chi = 0.2, \xi = 2, \gamma = 2, \theta = 1, \beta_1 = 0.5, \beta_2 = 0.5$. Table 1 shows the thermo-physical properties of Sodium Alginate (SA) third-grade fluid, magnesium oxide (MgO), and gold nanoparticles (Au). As a special case of our analysis, Table 2 provides a numerical comparison of Nusselt number and skin friction coefficient with previously published results [44,48-50] for varying values of the third-grade fluid parameter and Brinkman number. The numerical comparison of velocity and temperature profiles for simple third-grade fluid flow in the absence of a magnetic field and nanoparticles is shown in Tables 3 and 4. In Tables 3 and 4, the present results with homotopy perturbation method (HPM) are compared with different methods including Homotopy analysis method (HAM), Variational parameter method (VPM), and Galerkin's method (GM). However, most the results at each point are similar up to 3 decimal places. We can observe that the current results demonstrate very good correlation with previous studies and thereby confirm the validity of the hybrid nanofluid results.

Table 1: Thermophysical properties of Sodium Alginate third-grade fluid, magnesium oxide and gold nanoparticles [51-53].

Physical properties	Sodium Alginate (SA)	Gold (Au)	Magnesium oxide (MgO)
$\rho\left(kg/m^3\right)$	989	8908	3580
$\kappa\left(W/mK\right)$	0.6376	91	45
$C_p\left(J/kgK\right)$	4175	445	955
$\beta\left(1/K\right)$	0.00099	0.0000134	0.0000336
$\sigma\left(S/m\right)$	2.64×10^{-4}	1.7×10^{7}	2.6×10^{-6}

Table 2: Comparison of the present results with previously published results for skin friction and Nusselt number by considering $\psi_1 = \psi_2 = \gamma = \xi = \beta_1 = \beta_2 = 0.$

Physical parameters		Skin friction coefficient		Nusselt number	
$\varkappa$	δ	Rajagopal and Na [44]	Present results	Rajagopal and Na [44]	Present results
0.5	1	0.1628	0.1628	-0.4966	-0.4966
1	1	0.1592	0.1592	-0.4966	-0.4966
1	2	0.1593	0.1593	-0.4932	-0.4932
1	4	0.1596	0.1596	-0.4863	-0.4863
2	0.1	0.1532	0.1532	-0.4997	-0.4997
2	1	0.1533	0.1533	-0.4967	-0.4967

Table 3: Comparison of the present results with previously published results for velocity profile by considering $\psi_1 = \psi_2 = \gamma = \xi = \beta_1 = \beta_2 = 0.$

x	Present results	Ziabakhsh and Domairry [48]	Manshoor et al. [49]	Biswal et al. [50]
	HPM	HAM	VPM	GM
-1	0	0	0	0
-0.8	0.023919351	0.02391937	0.033923604	0.02368610
-0.6	0.032172695	0.03217274	0.032183540	0.03170120
-0.4	0.028406878	0.02840695	0.027143138	0.02794809
-0.2	0.016617651	0.01661778	0.016274634	0.01632954
0	0.000807628	0.00080780	0.000922405	0.00074834
0.2	-0.015082466	-0.01508225	-0.015143973	-0.01489272
0.4	-0.027103718	-0.02710348	-0.028257013	-0.02669087
0.6	-0.031230152	-0.03122988	-0.031223835	-0.03074332
0.8	-0.023429062	-0.02342875	-0.023274354	-0.02314729
1	0	0	0	0

Table 4: Comparison of the present results with previously published results for temperature profile by considering $\psi_1 = \psi_2 = \gamma = \xi = \beta_1 = \beta_2 = 0.$

x	Present results	Ziabakhsh and Domairry [48]	Manshoor et al. [49]	Biswal et al. [50]
	HPM	HAM	VPM	GM
-1	0.5	0.5	0.5	0.5
-0.8	0.400735884	0.40073588	0.400246306	0.40097357
-0.6	0.301177389	0.30117737	0.309367078	0.30172607
-0.4	0.201590913	0.20159090	0.201548465	0.20225927
-0.2	0.101927505	0.10192749	0.101925345	0.10257493
0	0.002060513	0.00206049	0.002174325	0.00267484
0.2	-0.098070046	-0.09807006	-0.098174536	-0.09743924
0.4	-0.198408504	-0.19840851	-0.198546725	-0.19776553
0.6	-0.298828514	-0.29882852	-0.298765434	-0.29830227
0.8	-0.399274729	-0.39927474	-0.400465233	-0.39904768
1	-0.5	-0.5	-0.5	-0.5

The graphical chart of the skin friction coefficient versus numerous values for key parameters is shown in Figure 2. The graphical chart of the Nusselt number profile for all emerging parameters is shown in Figure 3. Both figures are plotted with the assistance of equation (31) for MgO nanoparticle volume fraction ψ_1, gold nanoparticle volume fraction ψ_2, third-grade fluid parameter χ, Brinkman number δ, electric field strength parameter ξ Hartmann number γ, and buoyancy convection parameter θ. Figures 4 to 9 show the behavior of the velocity profile as a function of various parameters. Increment in third-grade fluid χ parameter tends to decelerate velocity in Figure 4, although the consequences are not significant. The results for Newtonian hybrid nanofluids are shown for $\chi = 0$. Figure 5 shows the variation of buoyancy convection parameter on velocity profile. The velocity profile is observed to be enhanced by the buoyancy convection parameter θ since thermal buoyancy force becomes more prominent as the thermal Grashof number rises, and therefore the velocity profile rises. Figure 6 shows that an increase in the Hartmann number γ has an opposing effect on fluid flow. With a stronger magnetic field there is a boost in the magnitude of Lorentz force which effectively impedes fluid motion. The maximum velocity is obtained by obtaining the non-magnetic case for $\gamma = 0$. Significant flow retardation is obviously obtained with higher magnetic parameters, which correlate to a larger transverse magnetic field presence in the regimes. Maximum velocity is always calculated at the center line (when $y = 0$), and the profiles are symmetric once again. Back flow is never generated in the region, even at the highest magnetic parameter of $\gamma = 4$, since the magnitudes of velocity are always positive. A comparable pattern has been seen for third-grade fluid motion in a

microchannel (Zhang et al. [54]). The variation of the nanoparticle particle volume fraction ψ_1 of MgO on the velocity profile is shown in Figure 7. It can be seen that when this nanoparticle is absent, the velocity is higher, and when it is present, the fluid flow is diminished. However, as illustrated in Figure 8, we can observe that increasing the nanoparticle volume fraction of the gold nanoparticles ψ_2 predicts similar results, but with a smaller amplitude of the velocity profile. The effects of electric strength ξ on the velocity profile are illustrated in Figure 9. It should be noted that the electric field strength has a substantial impact on the velocity profile. Since the electrical field is axial, with larger values of the electric field, the assistive electrical body force is boosted which aids momentum development and accelerates the channel flow.

The variation of the temperature profile in response to several significant parameters is depicted in Figures 10 to 16. Figures 10 and 11 show how the volume friction of MgO ψ_1 and Au ψ_2 nanoparticles vary with temperature. As can be observed in both graphs, the temperature profile is accentuated as the values of both variables increase. Since nanoparticles have a higher thermal conductivity than simple fluids $\psi_1 = \psi_2 = 0$, the impact of thermal diffusion is greater, therefore the temperature profile rises. Figure 12 shows that an increment in β_1 causes the temperature profile to decline. However, we can see in Figure 13 that higher values of β_2 boost the temperature profile. The variation of the Brinkman number δ on a temperature profile is shown in Figure 14. It is observed that Brinkman number significantly accelerates the temperature profile. In fact, viscous dissipation represents the conversion of mechanical energy into thermal energy via frictional effects-

higher value of Brinkman number therefore boost the temperature profile. The variation of the third-grade fluid parameter χ on the velocity profile is shown in Figure 15. The fluid parameter has a decreasing and minimal impact on the velocity profile as can be observed here. The variation of the Hartmann number γ on a temperature profile can be seen in Figure 16. The effects of the Hartmann number γ are insignificant closer to the channel walls, but the temperature profile rises in the core zone of the channel with elevation in the Hartmann number. The supplementary work expended in dragging the rheological nanofluid against the action of the transverse magnetic field is dissipated as thermal energy. This heats the core channel flow.

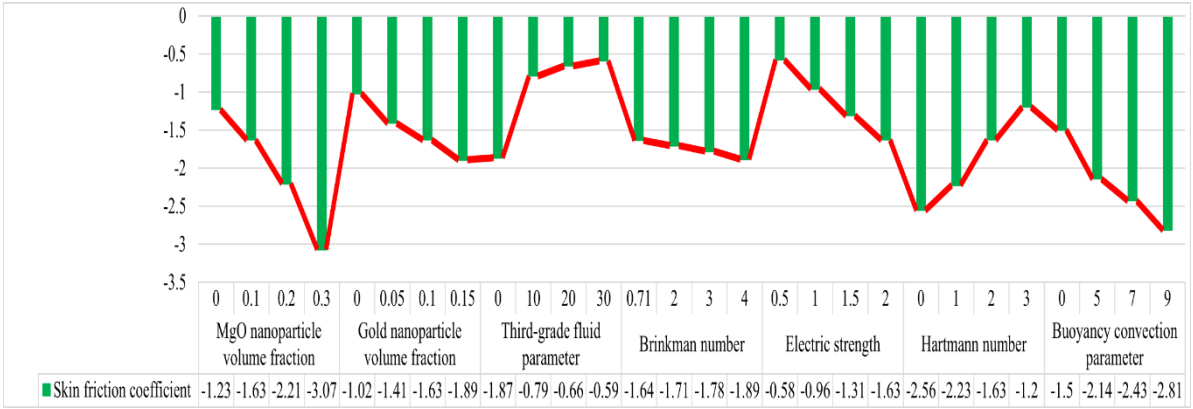

Figure 2: Skin friction coefficient profile for different values of MgO nanoparticle volume fraction ψ_1, Gold nanoparticle volume fraction ψ_2, third-grade fluid parameter χ, Brinkman number δ, Electric strength ξ, Hartmann number γ, and buoyancy convection parameter θ.

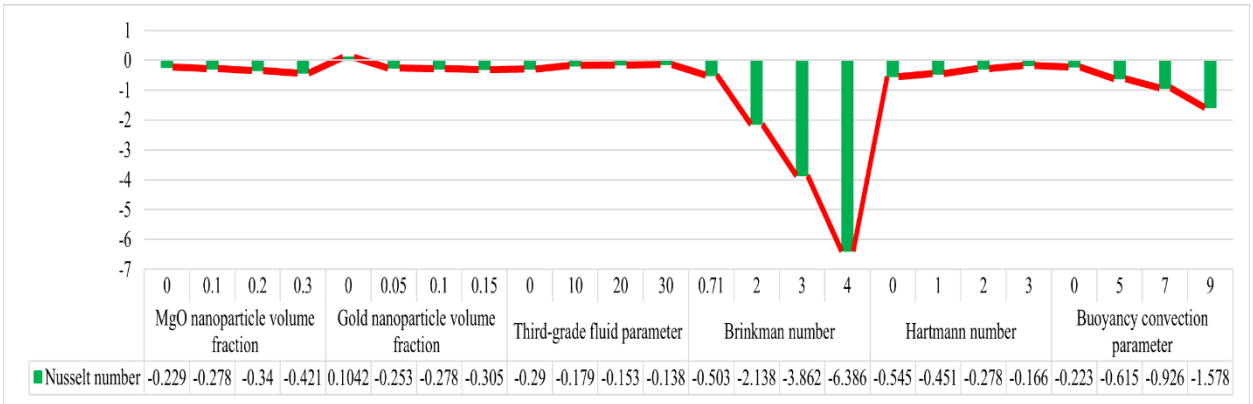

Figure 3: Nusselt number profile for different values of MgO nanoparticle volume fraction ψ_1, Gold nanoparticle volume fraction ψ_2, third-grade fluid parameter χ, Brinkman number δ, Electric strength ξ, Hartmann number γ, and buoyancy convection parameter θ

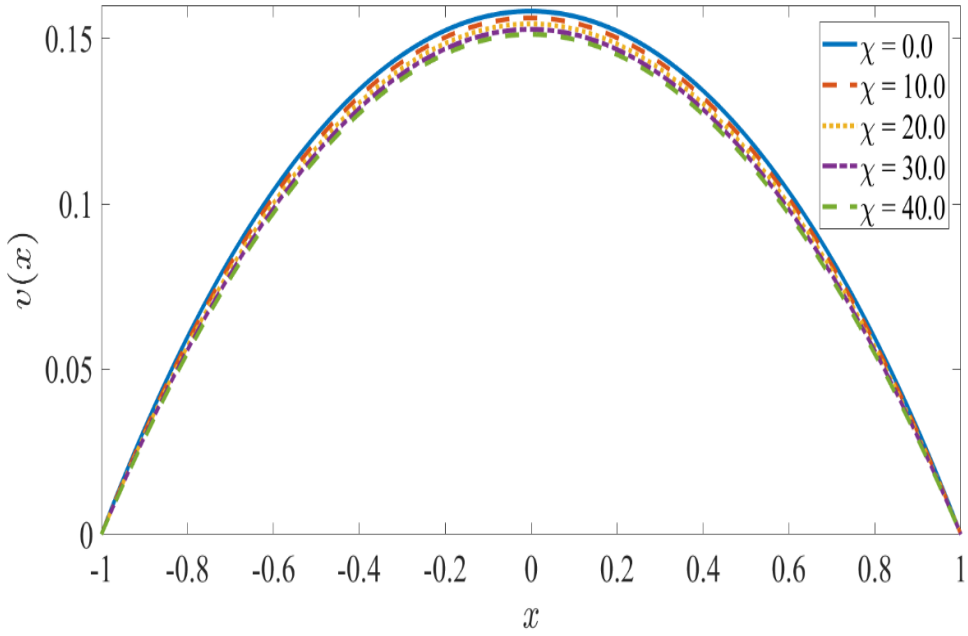

Figure 4: Effect of χ on velocity profile and $\delta = 0.5, \xi = 2, \gamma = 2, \theta = 1, \beta_1 = 0.5, \beta_2 = 0.5.$

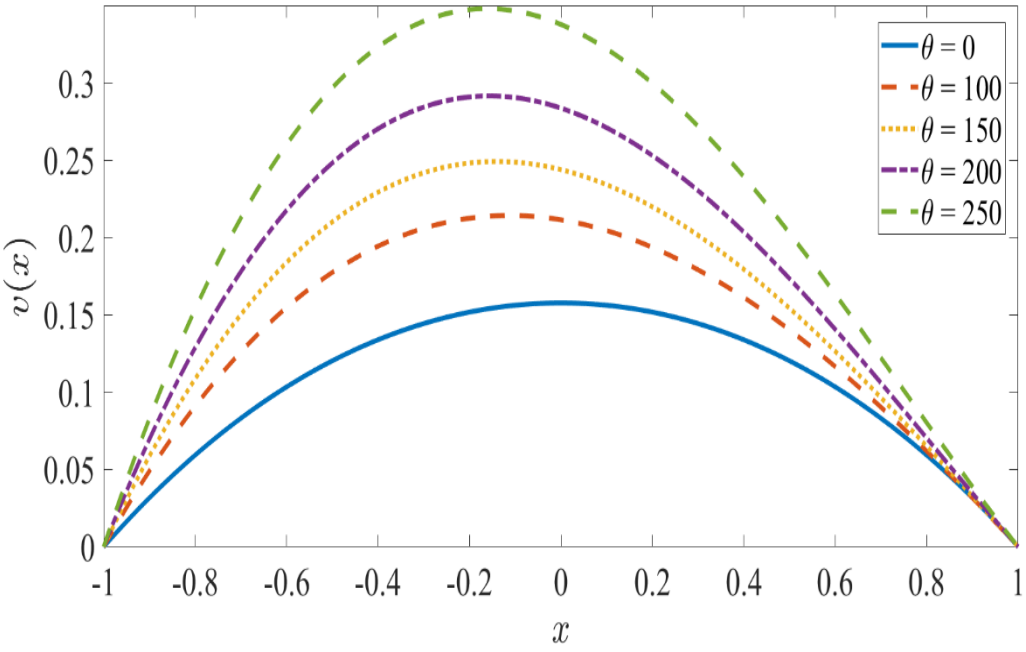

Figure 5: Effect of θ on velocity profile and $\delta = 0.5, \chi = 0.2, \xi = 2, \gamma = 2, \beta_1 = 0.5, \beta_2 = 0.5.$

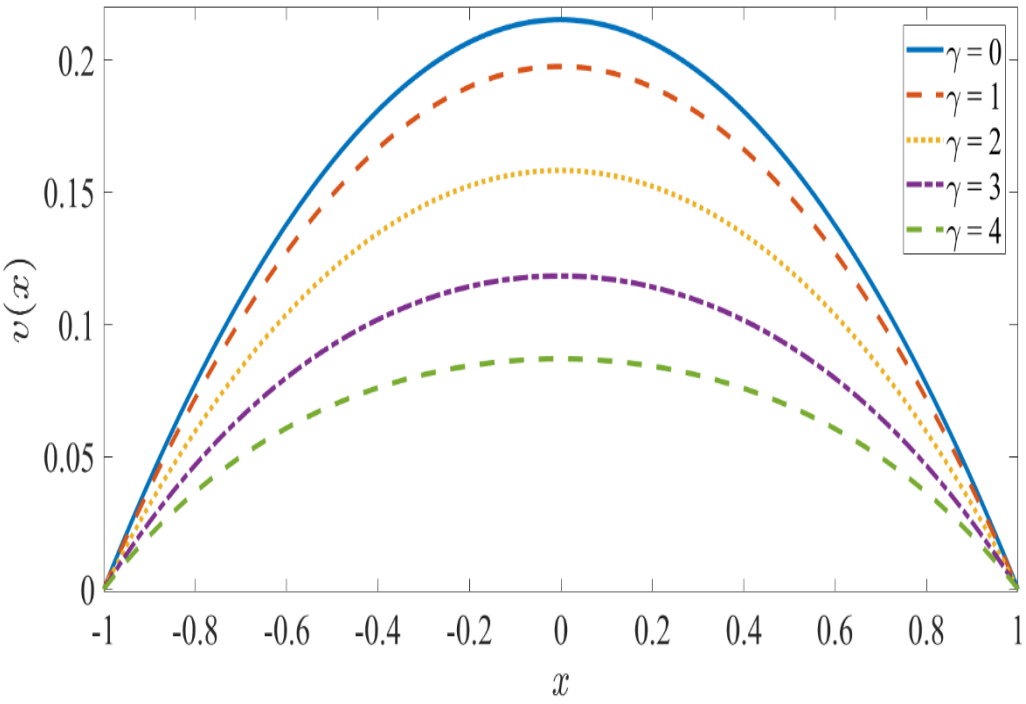

Figure 6: Effect of γ on velocity profile and $\delta = 0.5, \chi = 0.2, \xi = 2, \theta = 1, ; \beta_1 = 0.5, \beta_2 = 0.5.$

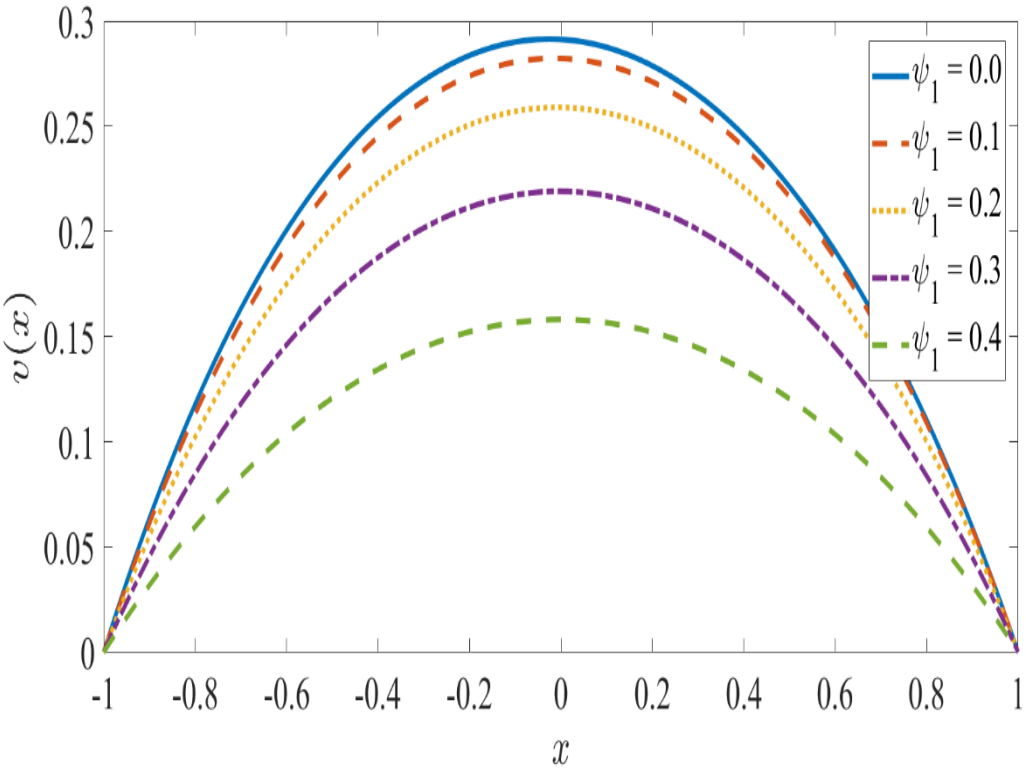

Figure 7: Effect of ψ_1 on velocity profile and
$\delta = 0.5, \chi = 0.2, \xi = 2; \gamma = 2, \theta = 1, \beta_1 = 0.5, \beta_2 = 0.5.$

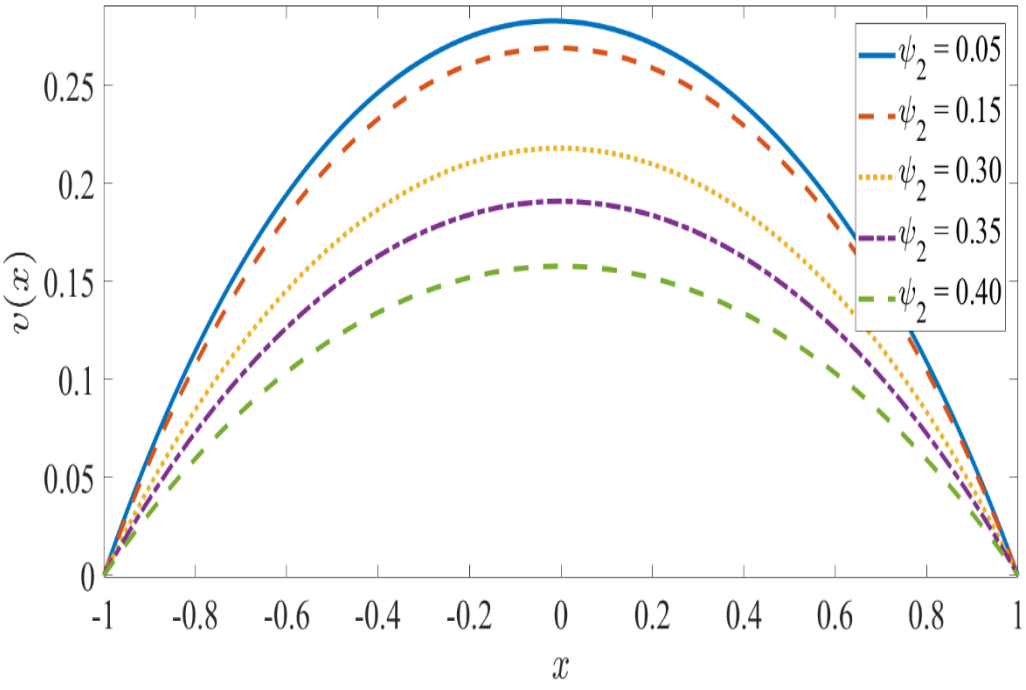

Figure 8: Effect of ψ_2 on velocity profile and
$\delta = 0.5, \chi = 0.2, \xi = 2, \gamma = 2, \theta = 1, \beta_1 = 0.5, \beta_2 = 0.5.$

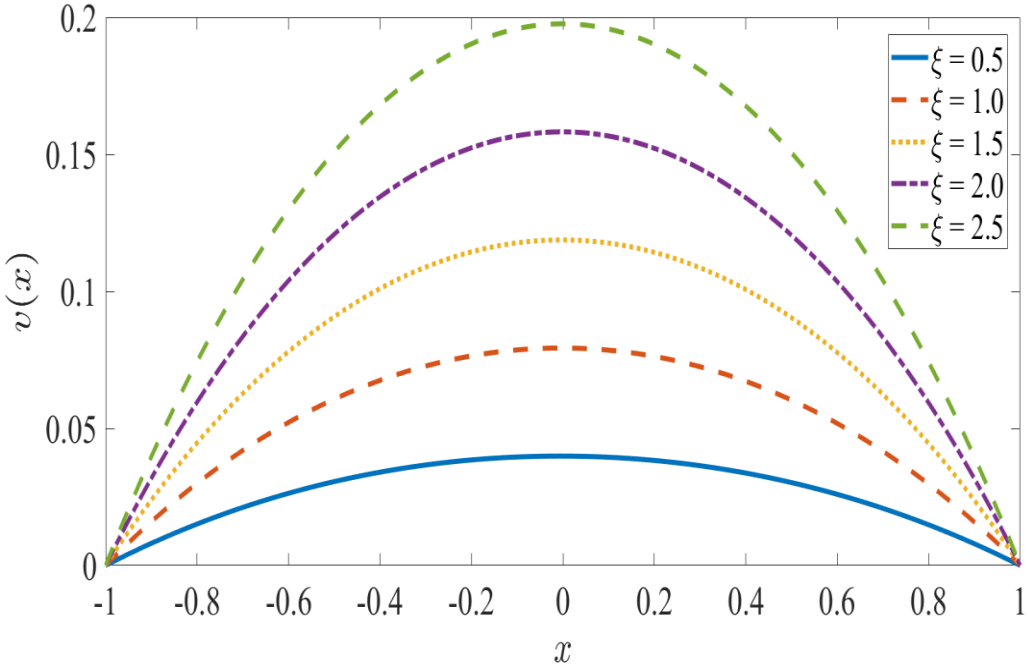

Figure 9: Effect of ξ on velocity profile and $\delta = 0.5, \chi = 0.2, \gamma = 2, \theta = 1, \beta_1 = 0.5, \beta_2 = 0.5.$

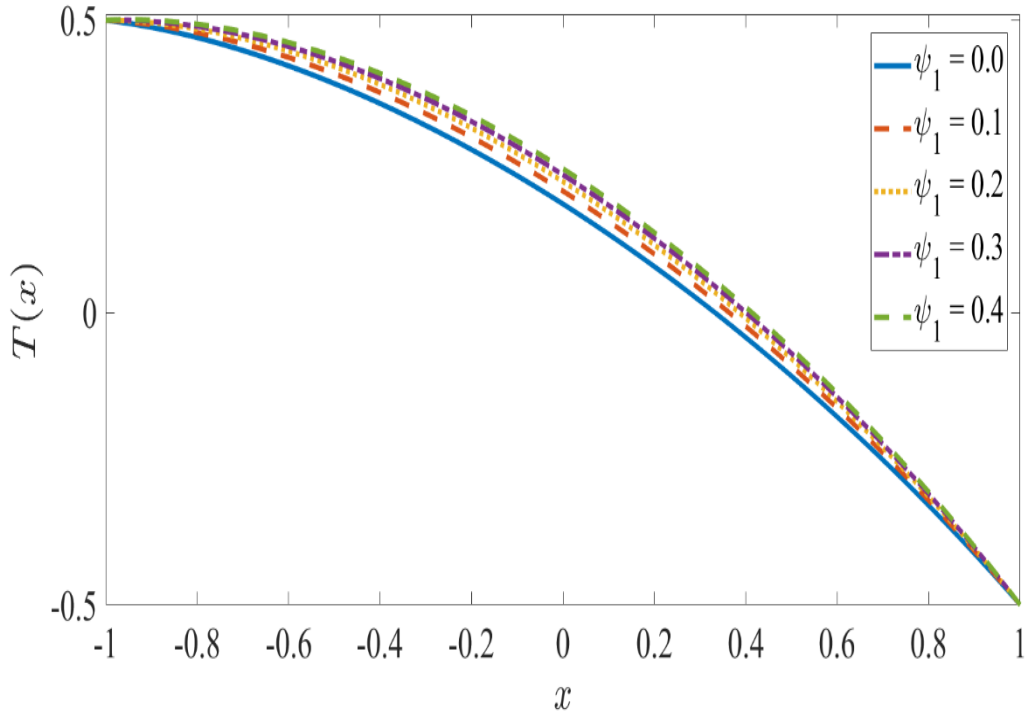

Figure 10: Effect of ψ_1 on temperature profile and
$\delta = 0.5, \chi = 0.2, \xi = 2, \gamma = 2, \theta = 1, \beta_1 = 0.5, \beta_2 = 0.5.$

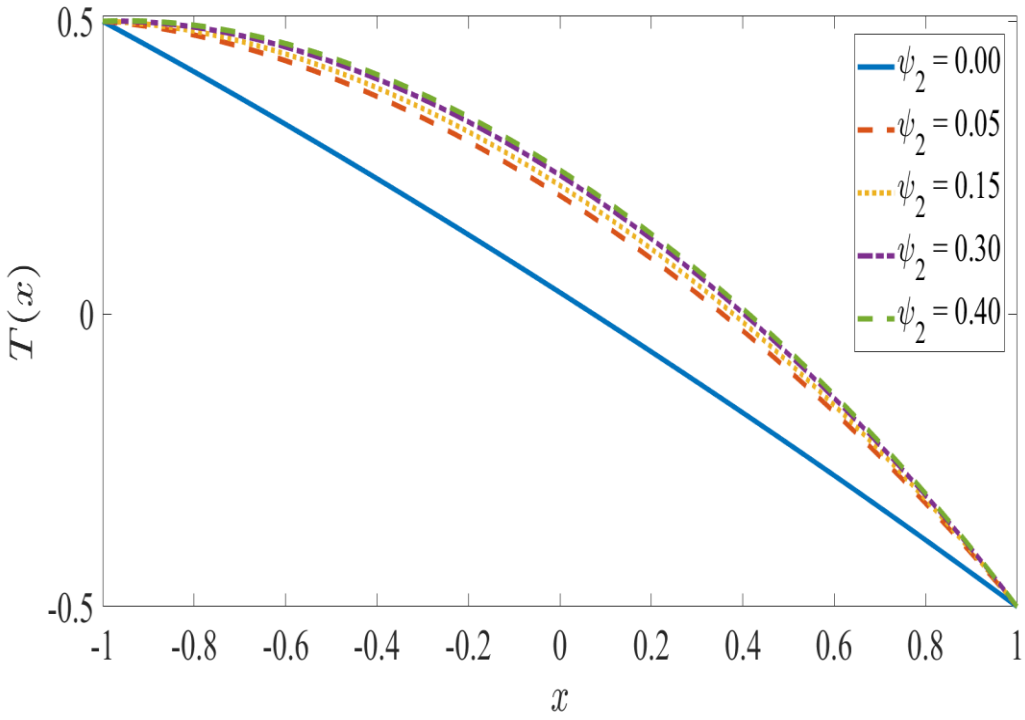

Figure 11: Effect of ψ_2 on temperature profile and $\delta = 0.5, \chi = 0.2, \xi = 2, \gamma = 2, \theta = 1, \beta_1 = 0.5, \beta_2 = 0.5.$

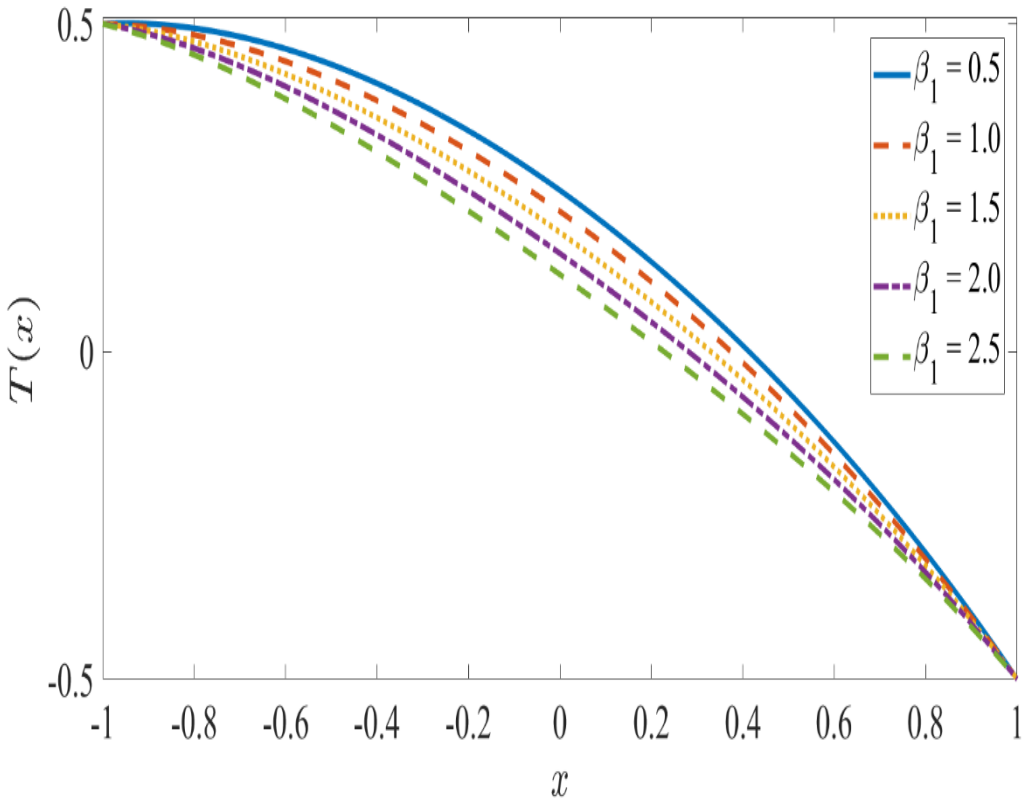

Figure 12: Effect of β_1 on temperature profile and $\delta = 0.5, \chi = 0.2, \xi = 2, \gamma = 2, \theta = 1, \beta_2 = 0.5.$

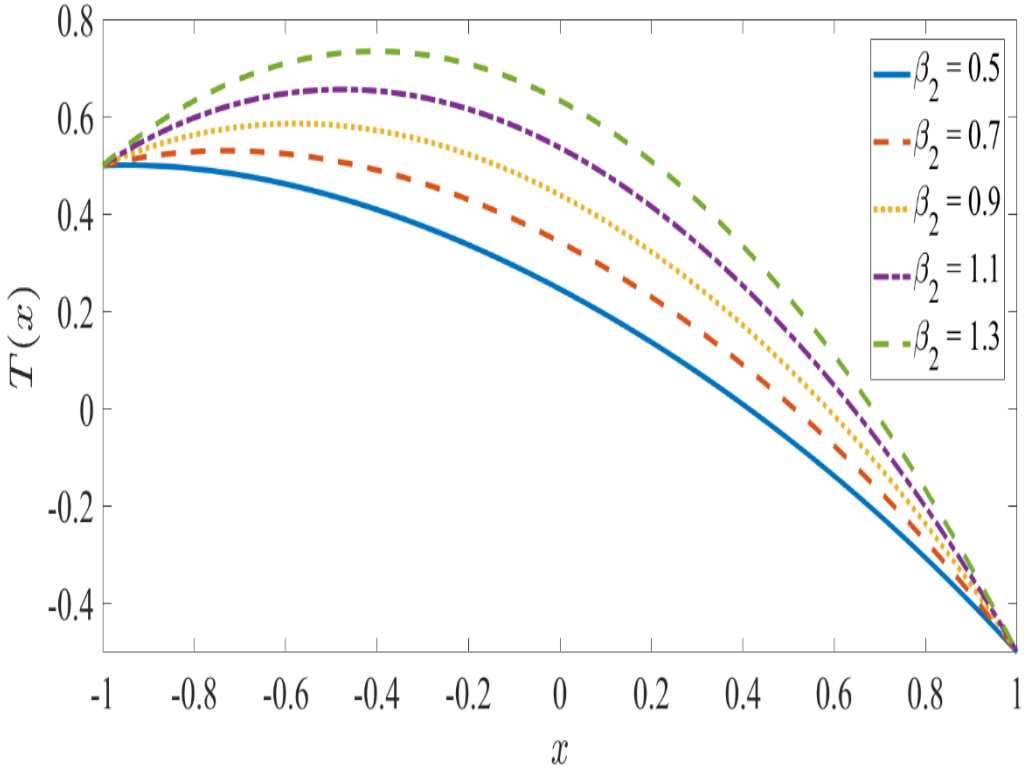

Figure 13: Effect of β_2 on temperature profile and $\delta = 0.5, \chi = 0.2, \xi = 2, \gamma = 2, \theta = 1, \beta_1 = 0.5.$

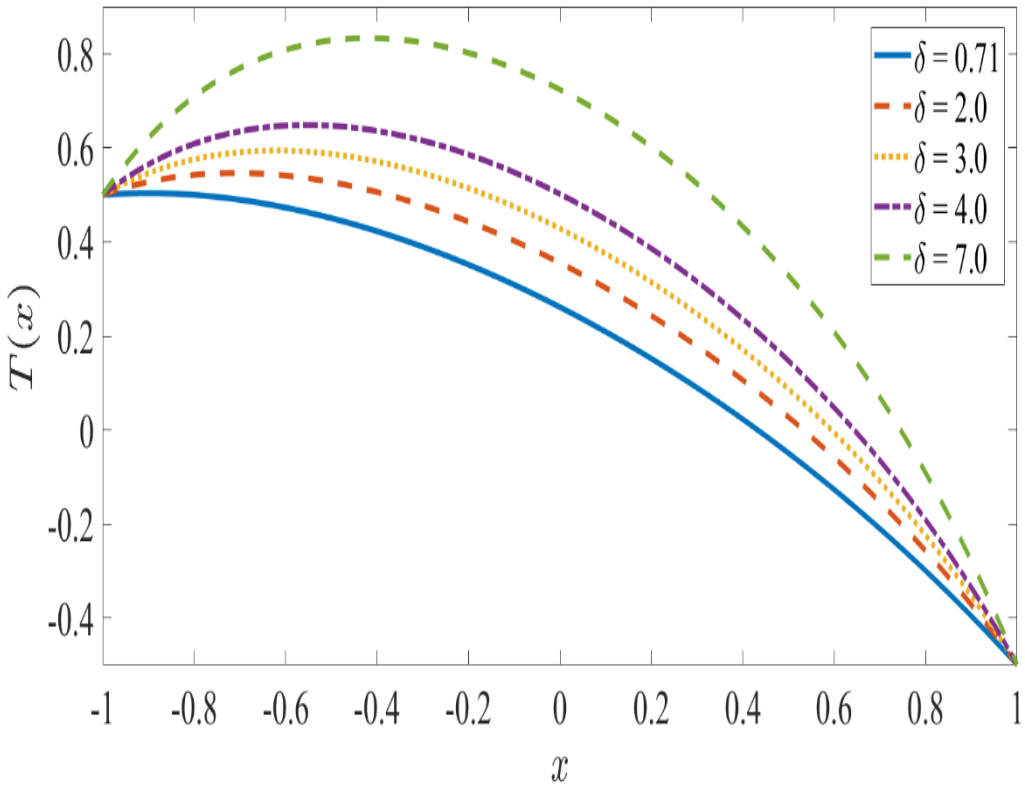

Figure 14: Effect of δ on temperature profile and $\chi = 0.2, \xi = 2, \gamma = 2, \theta = 1, \beta_1 = 0.5, \beta_2 = 0.5.$

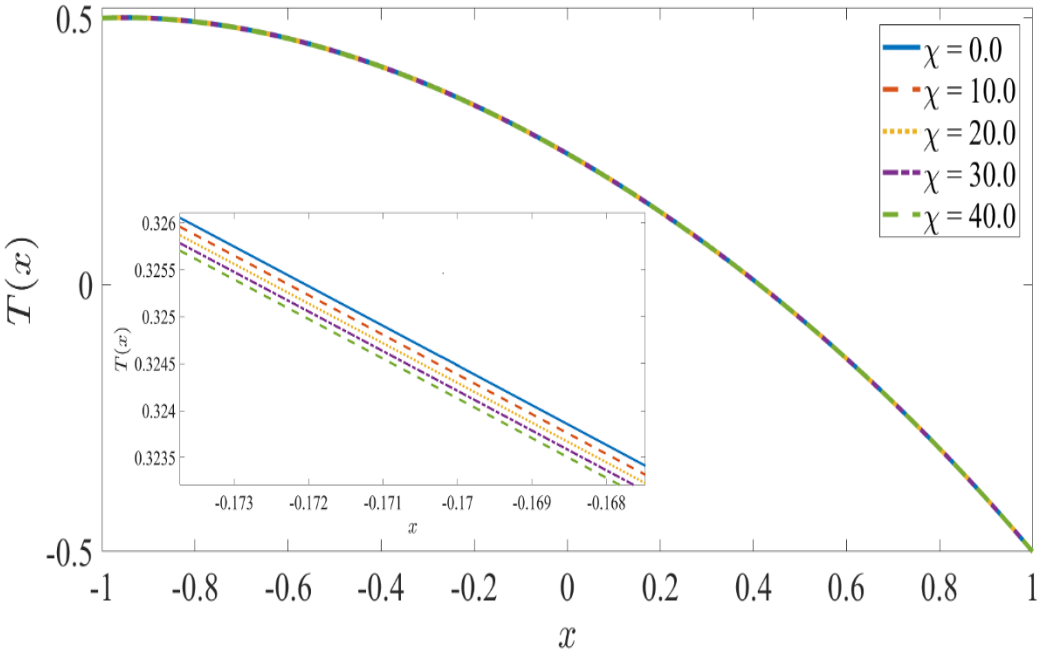

Figure 15: Effect of χ on temperature profile and $\delta = 0.5, \xi = 2, \gamma = 2, \theta = 1, \beta_1 = 0.5, \beta_2 = 0.5.$

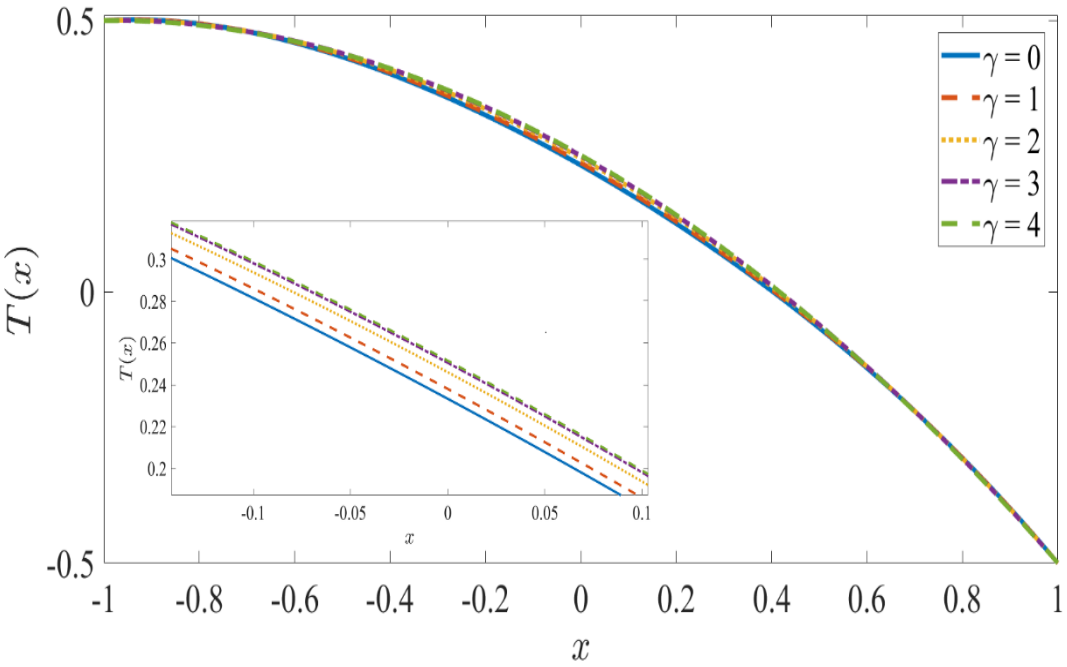

Figure 16: Effect of γ on temperature profile and $\delta = 0.5, \chi = 0.2, \xi = 2, \theta = 1, \beta_1 = 0.5, \beta_2 = 0.5.$

5. Conclusions

The electro-magnetohydrodynamic (EMHD) hybrid non-Newtonian electrically conducting and incompressible nanofluid flow with gold and magnesium oxide nanoparticles (Au/MgO-NPs) propagating between vertical parallel plates has been investigated. Sodium alginate third-grade base fluid is considered. Both an external transverse and axial electric field are considered. The solutions to the nonlinear differential equations with viable boundary conditions at the channel (duct) walls have been obtained using a perturbation technique. For each emerging parameter, both graphical and numerical results are presented. The key findings of the current analysis can be summarized as follows:

i. The rate of heat transfer of hybrid nanofluids is dramatically increased, and this is owing to an increase in the thermal conductivity of the fluid achieved with the combination of gold and magnesium oxide nanoparticles.

ii. Fluid motion is observed to be inhibited with an increment in third-grade fluid parameter, the magnetic field, and the nanoparticle volume fraction of both nanoparticles.

iii. With higher values of the buoyancy convection parameter and electric field strength parameter, the fluid velocity increased sharply i. e. strong flow acceleration is computed.

iv. The temperature magnitudes are significantly increased as the nanoparticle volume fraction of magnesium oxide and gold nanoparticles are increased.

v. The temperature profile is elevated with Brinkman number (viscous dissipation) and magnetic force, whereas increment in third-grade fluid parameter has a much weaker impact on the temperature profile.

vi. Very good correlation of the present solutions is achieved with special cases from the literature confirming the validity of the solution methodology deployed.

vii. The current research focused on *third-grade fluid* flow behavior. Future research could focus on the rheology of hybrid nanofluids using different non-Newtonian fluid models, as well as alternative nanoparticles, such as metal-based (zinc, silver, tantalum, etc.) and carbon-based (diamond, graphite, etc.) combinations (Zangeneh et al. [55]; Varmira et al. [56]; Bhatti and Abdelsalam [57]).

References

[1] F.P. Incropera, D.P. DeWitt, Fundamentals of heat and mass transfer, 5th ed., John Wiley & Sons, Nashville, TN, 2002.

[2] M. Potter, C.W. Somerton, Schaums outline of thermodynamics for engineers, 3rd ed., McGraw-Hill Professional, New York, NY, 2013.

[3] M. Ghalambaz, M. Sabour, S. Sazgara, I. Pop, R. Trâmbiţaş, Insight into the dynamics of ferrohydrodynamic (FHD) and magnetohydrodynamic (MHD) nanofluids inside a hexagonal cavity in the presence of a non-uniform magnetic field, J. Magn. Magn. Mater. 497 (2020) 166024.

[4] F. Selimefendigil, H.F. Öztop, A.J. Chamkha, MHD mixed convection and entropy generation of nanofluid filled lid driven cavity under the influence of inclined magnetic fields imposed to its upper and lower diagonal triangular domains, J. Magn. Magn. Mater. 406 (2016) 266–281.

[5] S. Rashidi, J.A. Esfahani, M. Maskaniyan, Applications of magnetohydrodynamics in biological systems-a review on the numerical studies, J. Magn. Magn. Mater. 439 (2017) 358–372.

[6] M. Marin, M.A. Othman, I. Abbas, An extension of the domain of influence theorem for generalized thermoelasticity of anisotropic material with voids, J. Comput. Theor. Nanosci. 12 (2015) 1594–1598.

[7] A. Hobiny, F. Alzahrani, I. Abbas, M. Marin, The effect of fractional time derivative of bioheat model in skin tissue induced to laser irradiation, Symmetry (Basel). 12 (2020) 602.

[8] M. Turkyilmazoglu, Equivalence of ratio and residual approaches in the homotopy analysis method and some applications in nonlinear science and engineering, Comput. Model. Eng. Sci. 120 (2019) 63–81.

[9] M. Sheikholeslami, D. Domiri Ganji, M. Younus Javed, R. Ellahi, Effect of thermal radiation on magnetohydrodynamics nanofluid flow and heat transfer by means of two phase model, J. Magn. Magn. Mater. 374 (2015) 36–43.

[10] S.U.S. Choi, J.A. Eastman, Enhancing thermal conductivity of fluids with nanoparticles (No. ANL/MSD/CP-84938; CONF-951135-29). Argonne National Lab. (ANL:Argonne, IL (United States). 1995.

[11] L. Xuan Hoang Khoa, I. Pop, M.A. Sheremet, Numerical simulation of solid and porous fins' impact on heat transfer performance in a differentially heated chamber, Mathematics. 10 (2022) 263.

[12] N.S. Gibanov, M.A. Sheremet, H.F. Oztop, K. Al-Salem, MHD natural convection and entropy generation in an open cavity having different horizontal porous blocks saturated with a ferrofluid, J. Magn. Magn. Mater. 452 (2018) 193–204.

[13] M.S. Astanina, M. Ghalambaz, A.J. Chamkha, M.A. Sheremet, Thermal convection in a cubical region saturated with a temperature-dependent viscosity fluid under the non-uniform temperature profile at vertical wall, Int. Commun. Heat Mass Transf. 126 (2021) 105442.

[14] K.G. Kumar, M.G. Reddy, P. Vijaya kumari, A. Aldalbahi, M. Rahimi-Gorji, M. Rahaman, Application of different hybrid nanofluids in convective heat transport of Carreau fluid, Chaos Solitons Fractals. 141 (2020) 110350.

[15] M. Gnaneswara Reddy, M.V.V.N.L. Sudha Rani, K. Ganesh Kumar, B.C. Prasannakumar, H.J. Lokesh, Hybrid dusty fluid flow through a Cattaneo–Christov heat flux model, Physica A. 551 (2020) 123975.

[16] M.G. Reddy, N. Kumar, B.C. Prasannakumara, N.G. Rudraswamy, K. Ganesh Kumar, Magnetohydrodynamic flow and heat transfer of a hybrid nanofluid over a rotating disk by considering Arrhenius energy, Commun. Theor. Phys. 73 (2021) 045002.

[17] S. Abinaya, H.P. Kavitha, M. Prakash, A. Muthukrishnaraj, Green synthesis of magnesium oxide nanoparticles and its applications: A review, Sustain. Chem. Pharm. 19 (2021) 100368.

[18] E. Kumaresan, A.G. Vijaya Kumar, B. Rushi Kumar, Chemically reacting on MHD boundary layer flow of CuO-water and MgO-water nanofluids past a stretching sheet in porous media with radiation absorption and heat generation/absorption, IOP Conf. Ser. Mater. Sci. Eng. 263 (2017) 062017.

[19] P. Pandiaraj, A. Gnanavelbabu, P. Saravanan, Experimental and statistical analysis of MgO nanofluids for thermal enhancement in a novel flat plate heat pipes, Int. J. Nanosci. 17 (2018) 1760018.

[20] H. Khodadadi, D. Toghraie, A. Karimipour, Effects of nanoparticles to present a statistical model for the viscosity of MgO-Water nanofluid, Powder Technol. 342 (2019) 166–180.

[21] M.S. Dehaj, M.Z. Mohiabadi, Experimental investigation of heat pipe solar collector using MgO nanofluids, Sol. Energy Mater. Sol. Cells. 191 (2019) 91–99.
[22] S. Choudhary, A. Sachdeva, P. Kumar, Investigation of the stability of MgO nanofluid and its effect on the thermal performance of flat plate solar collector, Renew. Energy. 147 (2020) 1801–1814.
[23] T. Hymavathi, J. Mathews, R.V.M.S.S. Kiran Kumar, Heat transfer and inclined magnetic field effects on unsteady free convection flow of MoS2 and MgO–water based nanofluids over a porous stretching sheet, Int. J. Ambient Energy. (2021) 1–9.
[24] M.G. Reddy, S.A. Shehzad, Molybdenum disulfide and magnesium oxide nanoparticle performance on micropolar Cattaneo-Christov heat flux model, Appl. Math. Mech. 42 (2021) 541–552.
[25] M. Sheikholeslami, M. Jafaryar, M.A. Sheremet, A. Shafee, Magnetic nanomaterial turbulent flow considering ferrohydrodynamics, in: Magnetic Nanoparticle-Based Hybrid Materials, Elsevier, 2021: pp. 209–230.
[26] M.A. Sheremet, M.M. Rashidi, Thermal convection of nano-liquid in an electronic cabinet with finned heat sink and heat generating element, Alex. Eng. J. 60 (2021) 2769–2778.
[27] S.M. Mousavi, M.N. Rostami, M. Yousefi, S. Dinarvand, I. Pop, M.A. Sheremet, Dual solutions for Casson hybrid nanofluid flow due to a stretching/shrinking sheet: A new combination of theoretical and experimental models, Chin. J. Phys. 71 (2021) 574–588.
[28] N. Khlebtsov, L. Dykman, Biodistribution and toxicity of engineered gold nanoparticles: a review of in vitro and in vivo studies, Chem. Soc. Rev. 40 (2011) 1647–1671.
[29] C.L.L. Beicker, M. Amjad, E.P. Bandarra Filho, D. Wen, Experimental study of photothermal conversion using gold/water and MWCNT/water nanofluids, Sol. Energy Mater. Sol. Cells. 188 (2018) 51–65.
[30] N.S. Elgazery, Flow of non-Newtonian magneto-fluid with gold and alumina nanoparticles through a non-Darcian porous medium, J. Egyptian Math. Soc. 27 (2019).
[31] S. Dinarvand, M. Nademi Rostami, An innovative mass-based model of aqueous zinc oxide–gold hybrid nanofluid for von Kármán's swirling flow: A comprehensive report on effects of nanoparticle shape factor, J. Therm. Anal. Calorim. 138 (2019) 845–855.
[32] U. Rashid, T. Abdeljawad, H. Liang, A. Iqbal, M. Abbas, M.J. Siddiqui, The shape effect of gold nanoparticles on squeezing nanofluid flow and heat transfer between parallel plates, Math. Probl. Eng. 2020 (2020) 1–12.
[33] M. Govindaraju, 1Department of Mathematics, Padmavani Arts and Science College for Women, M. Selvaraj, 2Department of Science and humanities, Ambal professional group of institutions, Boundary layer flow of Gold –thorium water based nanofluids over a moving semi-infinite plat, Res. Eng. Struct. Mater. (2020).
[34] J. Yin, X. Zhang, A. Hamid, Numerical investigation of thermal radiation impact on gold–molybdenum disulfide/water hybrid nanofluids with convective condition, Waves Random Complex Media. (2021) 1–19.
[35] S.K. Verma, A.K. Tiwari, S. Tiwari, D.S. Chauhan, Performance analysis of hybrid nanofluids in flat plate solar collector as an advanced working fluid, Sol. Energy. 167 (2018) 231–241.
[36] M. Ghalambaz, M. Sabour, I. Pop, D. Wen, Free convection heat transfer of MgO-MWCNTs/EG hybrid nanofluid in a porous complex shaped cavity with MHD and thermal radiation effects, Int. J. Numer. Methods Heat Fluid Flow. 29 (2019) 4349–4376.

[37] F. Saba, N. Ahmed, U. Khan, S.T. Mohyud-Din, A novel coupling of (CNT-Fe3O4/H2O) hybrid nanofluid for improvements in heat transfer for flow in an asymmetric channel with dilating/squeezing walls, Int. J. Heat Mass Transf. 136 (2019) 186–195.
[38] H.T. Basha, R. Sivaraj, I.L. Animasaun, Stability analysis on Ag-MgO/water hybrid nanofluid flow over an extending/contracting riga wedge and stagnation point, Comput. Therm. Sci. Int. J. 12 (2020) 491–508.
[39] L. Zhang, M.M. Bhatti, E.E. Michaelides, M. Marin, R. Ellahi, Hybrid nanofluid flow towards an elastic surface with tantalum and nickel nanoparticles, under the influence of an induced magnetic field, Eur. Phys. J. Spec. Top. 231 (2022) 521–533.
[40] M.M. Bhatti, M.B. Arain, A. Zeeshan, R. Ellahi, M.H. Doranehgard, Swimming of Gyrotactic Microorganism in MHD Williamson nanofluid flow between rotating circular plates embedded in porous medium: Application of thermal energy storage, J. Energy Storage. 45 (2022) 103511.
[41] M.R. Safaei, M. Safdari Shadloo, M.S. Goodarzi, A. Hadjadj, H.R. Goshayeshi, M. Afrand, S.N. Kazi, A survey on experimental and numerical studies of convection heat transfer of nanofluids inside closed conduits, Adv. Mech. Eng. 8 (2016) 168781401667356.
[42] M.I.A. Othman, S. Said, M. Marin, A novel model of plane waves of two-temperature fiber-reinforced thermoelastic medium under the effect of gravity with three-phase-lag model, Int. J. Numer. Methods Heat Fluid Flow. 29 (2019) 4788–4806.
[43] M.M. Bhatti, O.A. Bég, R. Ellahi, T. Abbas, Natural convection non-Newtonian EMHD dissipative flow through a microchannel containing a non-Darcy porous medium: Homotopy perturbation method study, Qual. Theory Dyn. Syst. 21 (2022).
[44] K.R. Rajagopal, T.Y. Na, Natural convection flow of a non-Newtonian fluid between two vertical flat plates, Acta Mech. 54 (1985) 239–246.
[45] M.M. Bhatti, R. Ellahi, M. Hossein Doranehgard, Numerical study on the hybrid nanofluid (Co3O4-Go/H2O) flow over a circular elastic surface with non-Darcy medium: Application in solar energy, J. Mol. Liq. 361 (2022) 119655.
[46] B. Takabi, S. Salehi, Augmentation of the heat transfer performance of a sinusoidal corrugated enclosure by employing hybrid nanofluid, Adv. Mech. Eng. 6 (2014) 147059.
[47] T. Tayebi, A.J. Chamkha, Entropy generation analysis during MHD natural convection flow of hybrid nanofluid in a square cavity containing a corrugated conducting block, Int. J. Numer. Methods Heat Fluid Flow. 30 (2020) 1115–1136.
[48] Z. Ziabakhsh, G. Domairry, Analytic solution of natural convection flow of a non-Newtonian fluid between two vertical flat plates using homotopy analysis method, Commun. Nonlinear Sci. Numer. Simul. 14 (2009) 1868–1880.
[49] B. Manshoor, M.F. Sies, I. Zaman, H.Z. Sharif, Natural heat convection through vertical flat plates by volume of parameter method, Journal of Complex Flow. 2 (2020) 27–31.
[50] U. Biswal, S. Chakraverty, B.K. Ojha, Natural convection of non-Newtonian nanofluid flow between two vertical parallel plates, Int. J. Numer. Methods Heat Fluid Flow. 29 (2019) 1984–2008.
[51] B. Sharma, S. Kumar, M.K. Paswan, Numerical investigation of MHD stagnation-point flow and heat transfer of sodium alginate non-Newtonian nanofluid, Nonlinear Eng. 8 (2019) 179–192.

[52] J.A. Rodrigo, M. Angulo, T. Alieva, Tailored optical propulsion forces for controlled transport of resonant gold nanoparticles and associated thermal convective fluid flows, Light Sci. Appl. 9 (2020) 181.
[53] M. Afrand, M. Hemmat Esfe, E. Abedini, H. Teimouri, Predicting the effects of magnesium oxide nanoparticles and temperature on the thermal conductivity of water using artificial neural network and experimental data, Physica E Low Dimens. Syst. Nanostruct. 87 (2017) 242–247.
[54] L. Zhang, M.M. Bhatti, E.E. Michaelides, Electro-magnetohydrodynamic flow and heat transfer of a third-grade fluid using a Darcy-Brinkman-Forchheimer model, Int. J. Numer. Methods Heat Fluid Flow. 31 (2021) 2623–2639.
[55] A. Zangeneh, A. Vatani, Z. Fakhroeian, S.M. Peyghambarzadeh, Experimental study of forced convection and subcooled flow boiling heat transfer in a vertical annulus using different novel functionalized ZnO nanoparticles, Appl. Therm. Eng. 109 (2016) 789–802.
[56] K. Varmira, M.M. Baseri, S. Khanmohammadi, M. Hamelian, A. Shahsavar, Experimental study of the effect of sheet-and-sinusoidal tube collector on the energetic and exergetic performance of a photovoltaic-thermal unit filled with biologically synthesized water/glycerol-silver nanofluid, Appl. Therm. Eng. 186 (2021) 116518.
[57] M.M. Bhatti, S.I. Abdelsalam, Bio-inspired peristaltic propulsion of hybrid nanofluid flow with Tantalum (Ta) and Gold (Au) nanoparticles under magnetic effects, Waves Random Complex Media. (2021) 1–26.

Author Statement: Investigation, Methodology and Writing – Original Draft Preparation, M. M. Bhatti; Conceptualization, O. A. Bég; Supervision and Writing—review and editing, validation. R.E.; validation, M. H. Doranehgard; Formal analysis, F. Rabiei. All authors have read and agreed to the published version of the manuscript.

Appendix A

$$\bar{v}_{2,0}=\frac{1}{20160\Im_1^2\Im_4}\left[\begin{array}{l}784\Im_1^2\Im_3\theta\delta+\Im_1\left\{\begin{array}{l}\Im_2\left(28\Im_3\theta\left(61\beta_1+150\beta_2\right)+\gamma^2\left(-4200\Im_4+739\Im_3\theta\delta\right)\right)\\+216\left(-140\Im_4+3\Im_3\theta\delta\right)\chi\end{array}\right\}\\-28\Im_4\left(61\Im_2^2\gamma^4+360\chi\left(3\xi+4\chi\right)+6\Im_2\gamma^4\left(25\xi+98\chi\right)\right)\end{array}\right], \tag{A1}$$

$$\bar{v}_{2,1}=\frac{\Im_3\theta\left(7\Im_2\gamma^2+96\chi\right)}{720\Im_1^2}, \tag{A2}$$

$$\bar{v}_{2,2}=\frac{\left[\begin{array}{l}-10\Im_1^2\Im_3\theta\delta+\Im_1\Im_2\left(60\Im_4\gamma^2-\Im_3\theta\left(25\beta_1+60\beta_2+11\gamma^2\delta\right)\right)\\-8\Im_1\Im_3\theta\delta\chi+5\Im_2\Im_4\gamma^2\left(5\Im_2\gamma^2+12\left(\xi+\chi\right)\right)\end{array}\right]}{240\Im_1^2\Im_4}, \tag{A3}$$

$$\bar{v}_{2,3}=-\frac{\Im_3\theta\left(\Im_2\gamma^2-12\chi\right)}{72\Im_1^2}, \tag{A4}$$

$$\bar{v}_{2,4}=\frac{1}{96\mathfrak{I}_1^2\mathfrak{I}_4}\left[\begin{array}{l}-2\mathfrak{I}_4\left(\mathfrak{I}_2\gamma^2+2\xi\right)\left(\mathfrak{I}_2\gamma^2-36\chi\right)\\+\mathfrak{I}_1\left(\mathfrak{I}_2\left(2\mathfrak{I}_3\theta\left(\beta_1+2\beta_2\right)+\varphi^2\left(-4\mathfrak{I}_4+\mathfrak{I}_3\theta\delta\right)\right)+144\mathfrak{I}_4\chi\right)\end{array}\right], \tag{A5}$$

$$\bar{v}_{2,5}=\frac{\mathfrak{I}_3\theta\left(\mathfrak{I}_2\gamma^2-72\chi\right)}{240\mathfrak{I}_1^2}, \tag{A6}$$

$$\bar{v}_{2,6}=\frac{\mathfrak{I}_2^2\mathfrak{I}_4\gamma^4-\mathfrak{I}_1\mathfrak{I}_2\mathfrak{I}_3\theta\left(\beta_1+\gamma^2\delta\right)-132\mathfrak{I}_2\mathfrak{I}_4\gamma^2\chi+2\left(\mathfrak{I}_1^2\mathfrak{I}_3\theta\delta+720\mathfrak{I}_4\chi^2\right)}{720\mathfrak{I}_1^2\mathfrak{I}_4}, \tag{A7}$$

$$\bar{v}_{2,0}=\frac{\mathfrak{I}_3\theta\delta\left(\mathfrak{I}_2\gamma^2+8\chi\right)}{6720\mathfrak{I}_1\mathfrak{I}_4}. \tag{A8}$$

Appendix B:

$$\bar{T}_{2,0}=-\frac{\delta\left(\begin{array}{l}3360\mathfrak{I}_1^2+\mathfrak{I}_2^2\left(1511\gamma^4+1708\gamma^2\beta_1\right)+384\chi\left(14\xi+15\chi\right)\\+56\mathfrak{I}_1\left(92\mathfrak{I}_2\gamma^2+75\mathfrak{I}_2\beta_1+60\xi+144\chi\right)\\+12\mathfrak{I}_2\left(308\gamma^2\xi+350\beta_1\xi+521\varphi^2\chi+392\beta_1\chi\right)\end{array}\right)}{20160\mathfrak{I}_1\mathfrak{I}_4}, \tag{B1}$$

$$\bar{T}_{2,1}=\frac{\mathfrak{I}_3\theta\delta\left(-14\mathfrak{I}_1+38\mathfrak{I}_2\gamma^2+49\mathfrak{I}_2\beta_1+72\chi\right)}{5040\mathfrak{I}_1\mathfrak{I}_4}, \tag{B2}$$

$$\bar{T}_{2,2}=\frac{\mathfrak{I}_2\left(\gamma^2+\beta_1\right)\delta\left(12\mathfrak{I}_1+5\mathfrak{I}_2\gamma^2+12\left(\xi+\chi\right)\right)}{48\mathfrak{I}_1\mathfrak{I}_4}, \tag{B3}$$

$$\bar{T}_{2,3}=\frac{\mathfrak{I}_3\theta\left(2\mathfrak{I}_1-\mathfrak{I}_2\left(\gamma^2+\beta_1\right)\right)\delta}{72\mathfrak{I}_1\mathfrak{I}_4}, \tag{B4}$$

$$\bar{T}_{2,4}=\frac{\delta\left(48\mathfrak{I}_1^2-12\mathfrak{I}_1\left(\mathfrak{I}_2\beta_1-4\xi\right)-\mathfrak{I}_2\left(\mathfrak{I}_2\left(11\gamma^4+6\gamma^2\beta_1\right)+12\left(\beta_1\xi+\gamma^2\left(2\xi+\chi\right)\right)\right)\right)}{288\mathfrak{I}_1\mathfrak{I}_4}, \tag{B5}$$

$$\bar{T}_{2,5}=\frac{\mathfrak{I}_3\theta\delta\left(-6\mathfrak{I}_1+\mathfrak{I}_2\left(2\gamma^2+\beta_1\right)+8\chi\right)}{240\mathfrak{I}_1\mathfrak{I}_4}, \tag{B6}$$

$$\bar{T}_{2,6}=\frac{\mathfrak{I}_2\gamma^2\delta\left(4\mathfrak{I}_1+\mathfrak{I}_2\left(7\gamma^2+\beta_1\right)+12\xi\right)+12\delta\left(24\mathfrak{I}_1+7A2\gamma^2-\mathfrak{I}_2\beta_1+16\xi\right)\chi}{720\mathfrak{I}_1\mathfrak{I}_4}, \tag{B7}$$

$$\bar{T}_{2,7}=-\frac{\mathfrak{I}_3\theta\delta\left(\mathfrak{I}_2\gamma^2+24\chi\right)}{504\mathfrak{I}_1\mathfrak{I}_4}, \tag{B8}$$

$$\bar{T}_{2,8}=-\frac{\delta\left(\mathfrak{I}_2\gamma^2-12\chi\right)\left(\mathfrak{I}_2\gamma^2+32\chi\right)}{1344\mathfrak{I}_1\mathfrak{I}_4}. \tag{B9}$$